Mon. Not. R. Astron. Soc. **350,** 1272–1287 (2004) doi:10.1111/j.1365-2966.2004.07607.x

The OH ground-state masers in W3(OH) – II. Polarization and multifrequency results

M. M. Wright,[1] M. D. Gray⋆[2] and P. J. Diamond[3]

[1]*H. H. Wills Physics Laboratory, University of Bristol, Tyndall Avenue, Bristol BS8 1TL*
[2]*Physics Department, UMIST, PO Box 88, Manchester M60 1QD*
[3]*Jodrell Bank Observatory, University of Manchester, Macclesfield SK11 9DL*

Accepted 2004 January 5. Received 2003 December 12; in original form 2003 July 16

ABSTRACT

We present observational data on OH masers in W3(OH) with the emphasis on the three ground-state lines, other than 1665 MHz, and on the polarization of the masers. Polarization studies indicate that the magnetic field orientation varies systematically over the field of view, and the large number of Zeeman pairs detected has allowed us to construct a map of the magnetic field in the source. In several parts of the region, the masers lie in arcs where the major axis of the maser usually lies parallel to the arc; these may delineate propagating shocks. A spectacular arc of maser emission occurs in the far south of the region at both 1665 and 1667 MHz. Such co-propagation of maser frequencies is very rare and exists only for pairs of lines where one line is 1665 MHz.

Key words: magnetic fields – masers – polarization – stars: formation – ISM: molecules – radio lines: ISM.

1 INTRODUCTION

We refer the reader to the general introduction in Paper I of this series (Wright, Gray & Diamond 2004) for information about the W3(OH) star-forming region, and to the observation section of the same work for details of the observations and data reduction. Unless stated otherwise, all data used in this paper were taken with the Very Long Baseline Array (VLBA), which is run by the National Radio Astronomy Observatory (NRAO) in the USA. Analysis of the 1665-MHz masers is also dealt with in Paper I, including an interpretation of their radial velocities and proper motions in terms of arotating disc, aligned approximately north–south and inclined at $\sim 10^{\circ}$ to the line of sight.

2 ANALYSIS OF W3(OH): 1667, 1612 AND 1720 MHz

2.1 1667-MHz masers

Fig. 1 shows the Stokes *I* spectrum of the maser fluxes calculated from the channel maps. The 1667-MHz maser spot map is shown in Fig. 2.

The 1667-MHz masers cover only the south-western sector of the continuum source. There are many fewer masers than at 1665 MHz; 41 are detected above a limiting flux density of 75 mJy, and the most intense masers have only 10 per cent of the intensity of the brightest masers seen at 1665 MHz. Immediately noticeable is the striking 'arc' of emission in the south of the map, which contains most of the maser flux.

Maser emission at 1667 MHz in W3(OH) has been studied by, for example, Mader, Johnston & Moran (1978), Norris & Booth (1981) and Fouquet & Reid (1982). Further observations were published by Norris, Booth & Diamond (1982), using the Multi-Element Radio Linked Interferometer Network (MERLIN) to observe at 1612, 1665 and 1667 MHz, detecting 15 masers at 1667 MHz. Unfortunately, absolute astrometry was not, at that time, routine with MERLIN, so the position was not accurately determined. Norris et al. (1982) had much lower spatial resolution than the current data, and made a mistake in assuming masers coincident in position and velocity at 1665 and 1667 MHz were truly physically coincident. Because the Zeeman splitting of 1667-MHz transitions is only 60 per cent of that of 1665-MHz transitions this is not a valid assumption to make. As a result of this, their 1667-MHz masers are positioned about 200 mas too far north-west with respect to the 1665-MHz masers. Finally, Gaume & Mutel (1987) observed W3(OH) with the Very Large Array (VLA) in 1985 January, although only for an observational period of ∼5 min. They detected 14 masers with a much lower positional accuracy than Norris et al. (1982), and their positional agreement is correspondingly poorer.

A sequence of three 1667-MHz observations, 1975 January (Mader et al. 1978), 1977 March (Norris & Booth 1981), and 1980 February (Fouquet & Reid 1982) found peak flux densities of, in chronological order, 15, 45 and then 15 Jy. These data suggest that the 1667-MHz masers flared on a time-scale of 2yr, before decaying to the original level on a similar time-scale. However,as the spectral shape in all three of these sets of observations is very similar, another very likely explanation is a flux miscalibration of the middle (1977)

⋆E-mail: Malcolm.Gray@umist.ac.uk

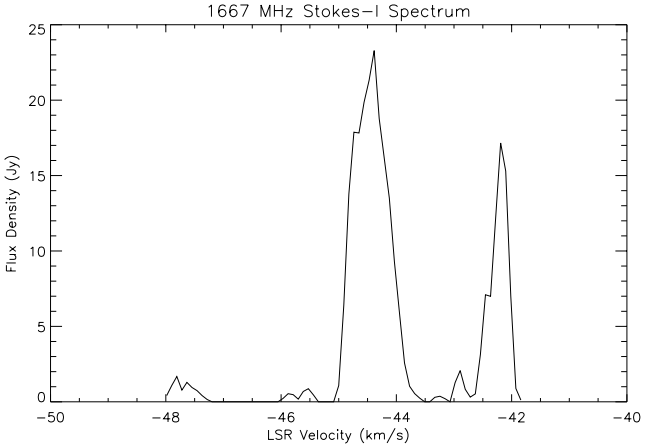

Figure 1. The Stokes *I* spectrum of the maser fluxes at1667 MHz, calculated from the channel maps.

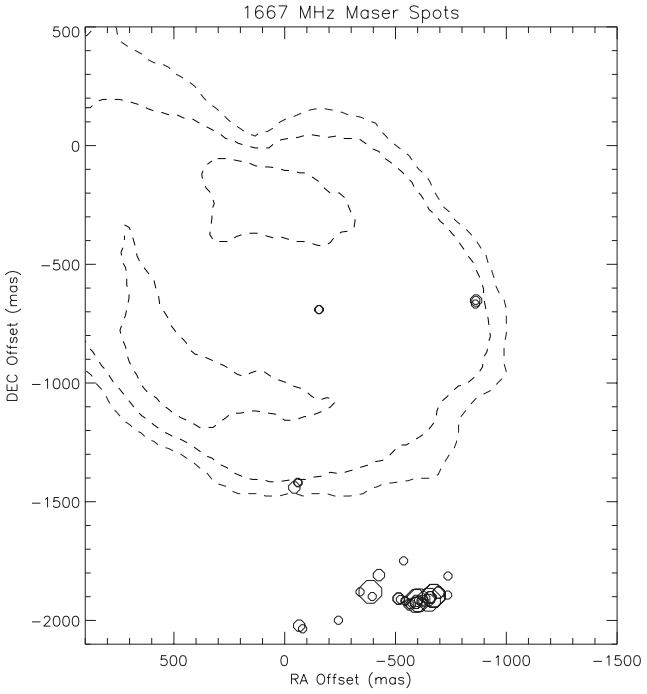

Figure 2. The 1667-MHz maser spot map. Contours are the 0.5, 7.1 and 16.6 mJy beam^{-1} levels of a VLA 2-cm continuum map (Masheder et al. 1994, and references therein). The spots are divided into three classes, represented by symbols of different sizes. In order of increasing symbol size, and maser flux, these classes are: (i) <0.4 Jy; (ii) 0.4–2.0 Jy; (iii) 2.0–10.0 Jy. The phase-centre of the magnitudes is at RA $02^{h}27^{m}03\overset{s}{.}825 \pm 0\overset{s}{.}001$, Dec. $+61^{\circ}52'25\overset{''}{.}089 \pm 0\overset{''}{.}01$ (J2000).

data set. The peak flux density measured by the present experiment is 23 Jy (see Fig. 1). The only concrete conclusion that can be drawn is that the right circular polarization (RCP) emission has halved in intensity with respect to the left circular polarization (LCP), whilst the velocity structure of the emission has remained simple.

2.2 Maser morphology at 1667 MHz

The southern arc feature in Fig. 2 is particularly striking; it contains over half of the 1667-MHz masers. The arc is just under 200 mas in extent, or ∼400 au at 2.2 kpc. The arc is shown in individual channels in Fig. 3. Channels 26–34 (Fig. 3a) are essentially RCP emission, covering a velocity range of −41.93 to −42.63 km s^{-1}, whilst channels 53–61 (Fig. 3b) are LCP emission with velocities between −44.30 and −45.00 km s^{-1}. Arcs and filaments are extremely rare in ground-state OH masers, although filamentary emission was seen in excited-state masers, at 13 GHz (Baudry & Diamond 1998), that overlie the 1665-MHz maser group *c*, as defined in our Paper I.

The 1667-MHz arc does not contain a velocity gradient so it is not an inclined disc. The arc is most likely a shock front propagating to the south. Support for this can be seen in the orientation of the maser position angles, which are aligned parallel to the arc (Fig. 3c).

Work by Elitzur et al. (1992) has shown that masers in shocks should be thin and planar, resembling discs with their planes parallel to the plane of the shock. They also suggest, however, that the true geometry of these masers may not be visible because of the beaming effects of saturation. The arc is evidence that the true geometry may in fact be visible. The 1665-MHz masers in this area (which actually overlap the 1667-MHz masers, see Section 3.1) are almost certainly moving south, as shown in fig. 12 of Paper I. The evolution and dissipation of this shock could be responsible for the maser activity here.

2.3 Polarization at 1667 MHz

This is the first very long baseline interferometry (VLBI) data set of 1667 MHz in W3(OH) which contains all polarization information. All of the masers are highly circularly polarized. Of the 41 masers detected, 22 (54 per cent) were LCP and 19 (46 per cent) RCP. 80 per cent of the masers have over 90 per cent circular polarization. Indeed, only four masers have less than 75 per cent circular or total polarization, and these four masers are notable. Two of them are faint and are highly blueshifted at the extreme south of the map. Of the other two, one is the most intense maser at 1667 MHz and the other is a close companion. The most intense maser is twice as intense as the second maser, and is the only maser with a significant intensity of linear polarization; it has 0.92 Jy of linear flux, compared to the next strongest at 0.11 Jy. The remainder have linear fluxes below 0.1 Jy. In contrast to results at 1665 MHz, at 1667 MHz there is no strong variation in the strength of polarization across the map. This may well be because the 1667-MHz masers do not cover enough of W3(OH) for very significant variations to become apparent. The polarization angle varies gradually through 90° along the line shape of the brightest maser (Fig. 4a). This is the only 1667-MHz maser for which the linear flux is strong enough to give reliable polarization angle measurements, but comparing it to masers at 1665 MHz, we see that this angle change is unusual behaviour – polarization angles, where they are reliable, are generally stable across the maser line shape (Fig. 4b). The effect we observe could be caused by a change in the magnetic field direction within the propagation path of the maser. This is more likely than Faraday rotation because of the high free electron density needed for Faraday effects within a maser.

2.4 Line shapes at 1667 MHz

The 1667-MHz maser line shapes were typically well fitted by Gaussians. The average FWHM of the Gaussian-fit 1667-MHz masers is ∼240 m s^{-1} (Table 1), compared to that of the 1665-MHz masers of ∼280 m s^{-1}. This is the lowest value of all the ground-state lines. This is as would be expected from the modelling by Gray, Field & Doel (1992), which suggested that 1667-MHz masers require lower velocity shifts over their propagation length. In the models by Gray et al. (1992) most of the parameter space in which 1667 MHz emerges as the dominant maser is concentrated in velocity shifts for the pumping lines <0.8 km s^{-1}, kinetic temperatures in the range 50–75 K, and OH number densities between 25 and 60 cm^{-3}. Although

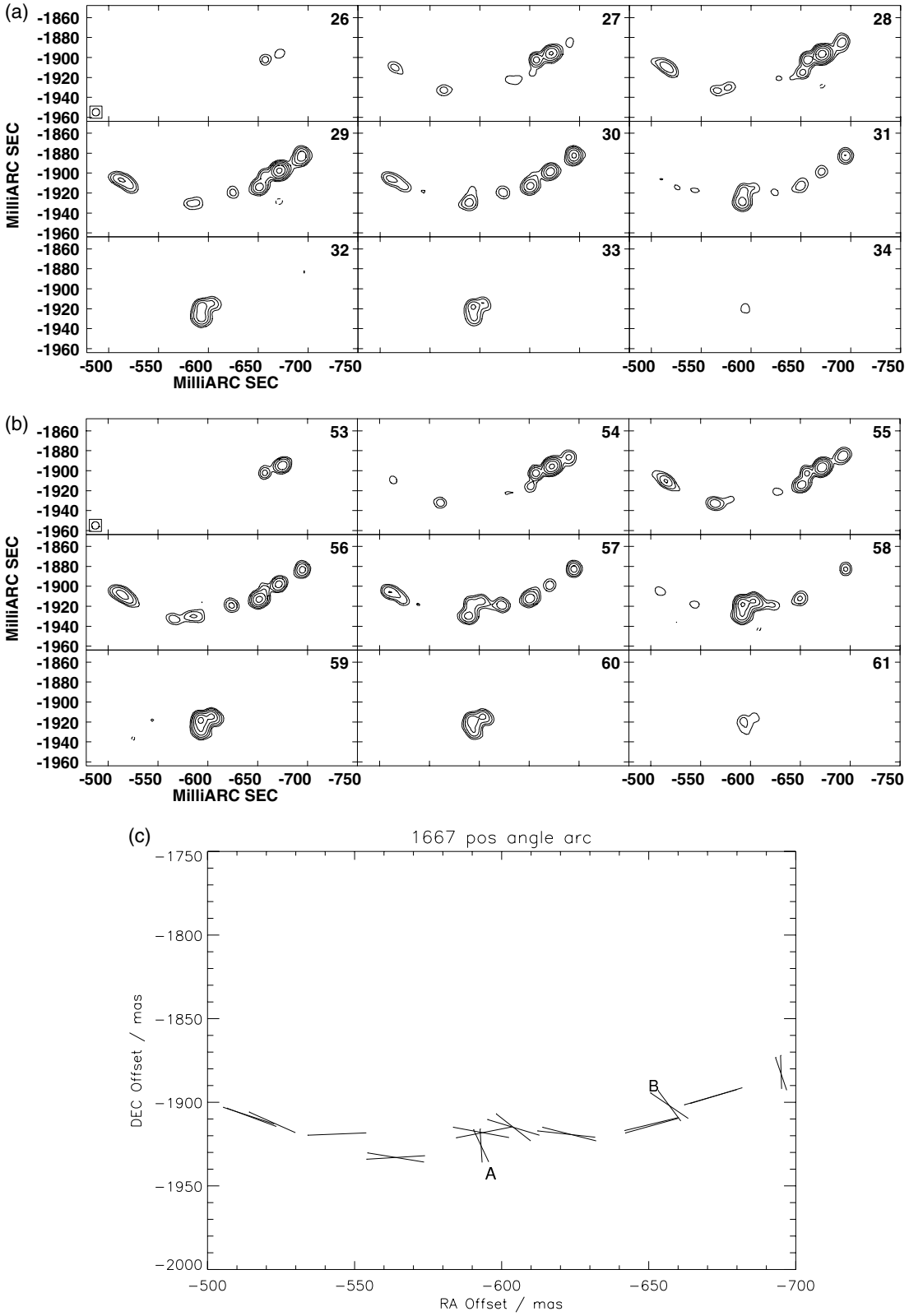

Figure 3. Channel maps of the southern arc feature at 1667 MHz. (a) shows channels 26–34 inclusive, corresponding to the RHC polarized emission. (b) shows the LHC polarized features in channels 53–61 inclusive. (c) shows the position angles of the masers in the arc feature. Note the occurrence of Zeeman pairs, which give the appearance of 'crosses'. Masers A and B are in complex areas of overlapping emission, where position angles computed from Gaussian fitting are unreliable.

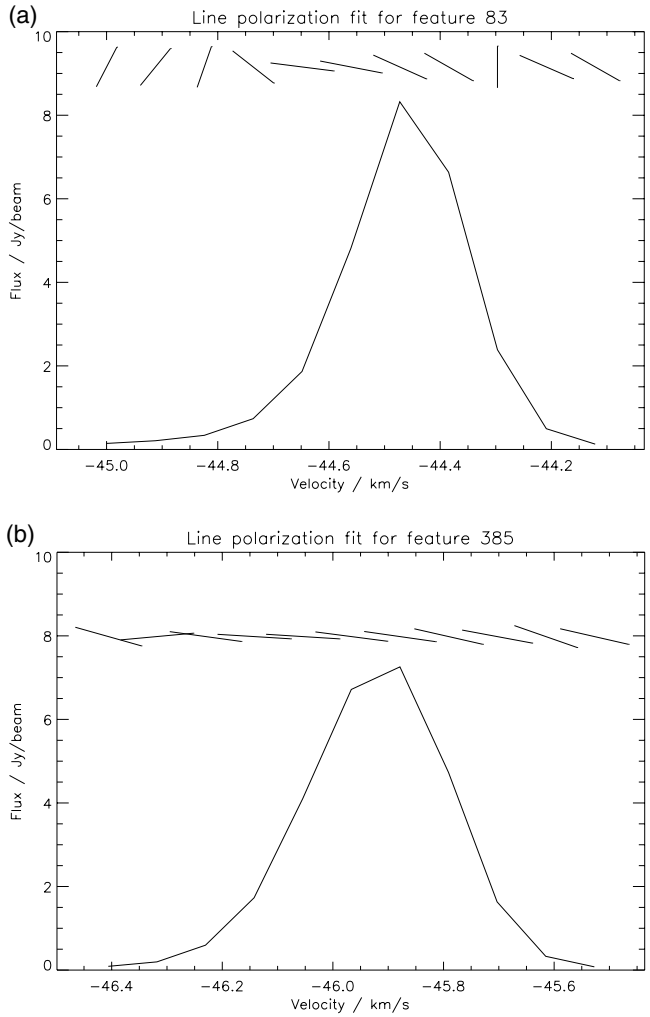

Figure 4. In (a), we show the variation of the polarization angle across the line shape of feature 83, the brightest feature at 1667 MHz. A typical 1665-MHz line shape (feature 385) is shown in (b), where the polarization angle changes little with velocity.

Table 1. Mean linewidths at FWHM for the four ground-state transitions, and the associated standard deviations. The asterisked column shows the results for 1720 MHz if the very broad feature (width = 509 m s^{-1}) is excluded.

Frequency (MHz)	1612	1665	1667	1720	1720*
Mean FWHM (ms^{-1})	275	281	241	299	257
Standard deviation (ms^{-1})	77	59	58	108	37

1665-MHz masers generally favour slightly hotter gas, and higher [OH] concentrations, the main distinguishing parameter is velocity shift; significantly larger (several km s^{-1}) shifts in the pumping lines are required because the 1665-MHz pumping scheme requires far-infrared line overlap. Maser gain lengths can be much shorter than the 'overlap length' used in the models, but some broadening of 1665-MHz lines, relative to 1667 MHz, would be expected on the basis of larger velocity shifts over a typical maser gain length. The 1667-MHz lines could also be narrower because, on average, they are less saturated with consequently reduced rebroadening.

2.5 Magnetic field and velocity structure at 1667 MHz

14 Zeeman pairs were found; they are listed in Table 2. A 1667-MHz maser, from our sample, has a 68 per cent chance of being in a Zeeman pair. However, in the arc feature, 22 of the 23 masers are in Zeeman pairs. This much higher incidence of Zeeman pairs probably indicates very much lower velocity shifts in the line of sight within the arc compared with masers elsewhere in the source. Such lower line-of-sight velocity shifts would be expected in a shock expanding to the south.

The median ratio of the fluxes of the Zeeman pairs is 1.7 : 1, and the mean is 2.1 : 1. Thus, the Zeeman pairs are much more even in intensity than at 1665 MHz. The uniformity of the field in the arc indicates a constant density on a scale of 400 au in the arc. One maser feature exhibits a field strength of 2.4 mG; this value is much lower than for any maser at 1665 MHz and, surprisingly, is also lower than the value of the field in the surrounding gas, given in Güsten, Fiebig & Uchida (1994), of 3.2 mG. This maser may lie in gas that is actually less dense than much of the cloud in this region. Such low fields were proposed by Bloemhof et al. (1992) at 1665 MHz, but not reproduced in this work at that frequency; they were also proposed by Desmurs et al. (1998) at 6 GHz in W3(OH). The range of field strengths is however still in good agreement with other 1667-MHz measurements in Gaume & Mutel (1987), and in Norris et al. (1982) whose proposed Zeeman pair would have a field of about 6 mG.

The blueshifted masers in the extreme south do not have a Zeeman partner to deduce their demagnetized velocity, but if their magnetic field strength is in the typical range then they are probably not part of the same bulk movement as the rest of the 1667-MHz masers. This will be examined more in Section 3.3, when the different frequencies are compared.

2.6 1612-MHz masers

Fig. 5 shows the Stokes *I* spectrum of the maser fluxes calculated from the channel maps. The maser spectrum also shows a very weak but notable blueshifted maser feature at -47.5 km s^{-1}.

The 1612-MHz maser map is shown in Fig. 6. As can be readily seen, the 1612-MHz masers are divided into two groups: the brighter masers in the north and a line of weaker masers strung out in the south. The northern masers lie within the contours of continuum emission, which defines the UCH II region, whilst the southern masers lie well outside these contours.

The first interferometer study of 1612 MHz in W3(OH) was in 1982, when both Norris et al. (1982) and Fouquet & Reid (1982) published multifrequency observations. Fouquet and Reid had very poor sensitivity in their observation with three US antennas, and did not list their fluxes, although their 1720- and 1612-MHz positions match well with subsequent data. Norris et al. (1982) observed at 1612, 1665 and 1667 MHz with MERLIN in 1980–81. The 1612-MHz transition was observed only in RCP. They detected only two masers at 1612 MHz, which they positioned on a map by assuming the maser which was coincident in velocity with a maser in their 1667-MHz map was also coincident in position. For a variety of reasons including Zeeman effects, this was not a valid assumption to make. Gaume & Mutel (1987) also studied 1612-MHz masers in W3(OH) with the VLA in 1985 January, although only for an observational period of ∼5 min. More recent VLA data at 1612 MHz have been published by Argon, Reid & Menten (2000). Comparing spectra with the single-dish spectrum of Norris et al. (1982) indicates that

Table 2. 1667-MHz Zeemanpairs. Information for peak flux, RA and Dec. are from the peak channel in the brighter of the two Zeeman components. Quality code 'a' implies a Zeeman component separation of less than 6 mas; quality 'b' implies a separation between 6 and 12 mas. These codes are also used inTables 4 and 5.

Peak flux density (Jy beam^{-1})	RA offset (mas)	Dec. offset (mas)	Magnetic field (mG)	Magnetic field error ±(mG)	Demagnetized velocity (km s^{-1})	Demagnetized velocity error ±(km s^{-1})	Pair quality	Location
0.41	−863.8	−652.5	2.43	0.18	−45.10	0.03	a	East
1.98	−694.5	−1882.4	6.58	0.17	−43.42	0.03	a	Arc
4.92	−671.4	−1896.6	6.45	0.14	−43.28	0.03	a	Arc
1.55	−656.8	−1902.4	6.59	0.17	−43.25	0.03	a	Arc
2.16	−651.4	−1913.0	6.62	0.16	−43.39	0.03	a	Arc
0.74	−622.4	−1918.9	6.77	0.16	−43.43	0.03	a	Arc
2.02	−603.9	−1914.9	6.36	0.17	−43.67	0.03	a	Arc
3.69	−592.8	−1917.7	6.57	0.14	−43.63	0.02	a	Arc
1.90	−592.7	−1925.9	6.67	0.18	−43.59	0.03	a	Arc
0.71	−564.2	−1932.8	6.95	0.18	−43.24	0.03	b	Arc
0.13	−544.5	−1919.1	6.70	0.18	−43.55	0.03	b	Arc
1.20	−514.7	−1908.7	6.74	0.17	−43.37	0.03	a	Arc
0.23	−155.2	−690.3	4.22	0.18	−44.78	0.03	b	Centre
0.26	−58.6	−1418.1	4.22	0.18	−43.55	0.03	b	Centre

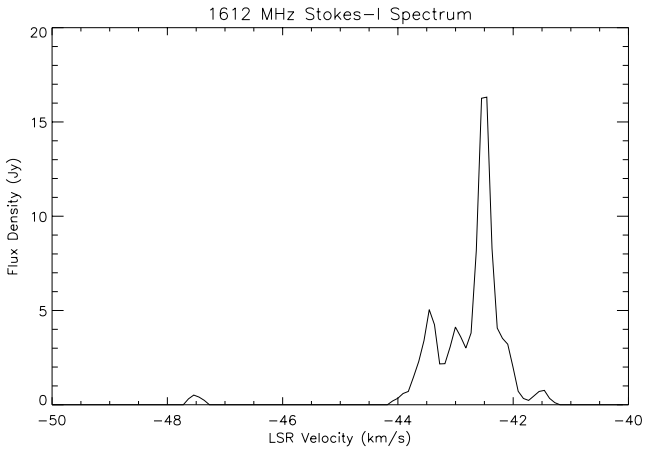

Figure 5. The Stokes *I* spectrum of the maser fluxes at1612 MHz, calculated from the channel maps.

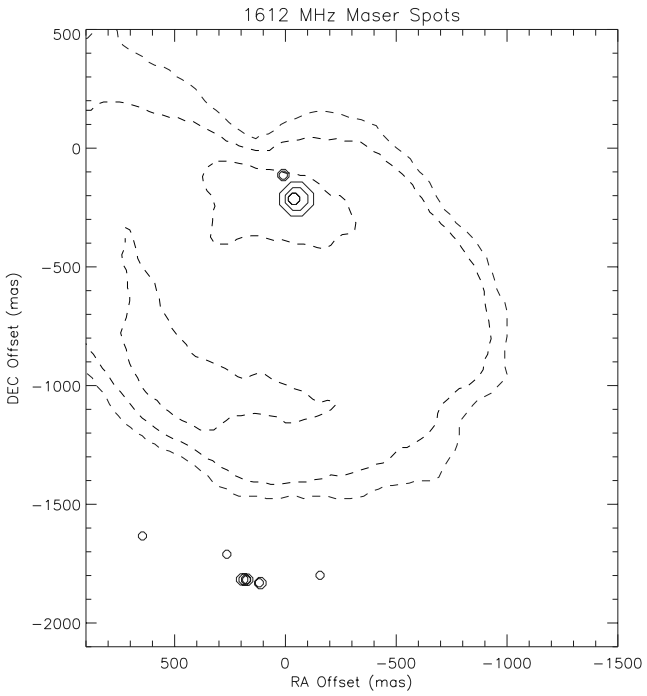

Figure 6. The 1612-MHz maser spot map. Contours are the 0.5, 7.1 and 16.6 mJy beam^{-1} levels of a VLA 2-cm continuum map (Masheder et al. 1994, and references therein). The spots are divided into four classes, represented by symbols of different sizes. In order of increasing symbol size, and maser flux, these classes are: (i) <0.4 Jy; (ii) 0.4–2.0 Jy; (iii) 2.0–10.0 Jy; (iv) >10 Jy.

the emission has remained qualitatively the same in the 16 years since their observation, with the main peak at −42.5 km s^{-1}.

Turning now to the maps, Norris et al. (1982) detected only two masers, separated by just under 100 mas. This means that they can only have detected either the northern or the southern cluster. An inspection of velocities indicates that, surprisingly, they only detected the southern emission – and have placed it ∼800 mas too far west with respect to the continuum by aligning the peak with the brightest 1665-MHz maser. The masers in the current work are weaker by a factor of 3. This is probably the result of resolving out slightly diffuse emission – the channel maps of these features show that they are well resolved, with major axes >4.13 mas – although an additional decline in brightness cannot be ruled out. The present intensity of the northern emission would certainly have made it detectable at the time of the Norris et al. observations, and their single-dish spectrum does show a peak at the −42.5 km s^{-1} velocity of the RCP northern feature. It is not clear what the presence of the −42.5 km s^{-1} peak in the total power spectrum represents if it is not the northern feature.

The VLA observations by Gaume & Mutel (1987) had much poorer spatial resolution and velocity resolution (only 1.1 km s^{-1}) than the present work or that of Norris et al., but their sensitivity was better than that of Norris et al., having a 1σ noise of ∼30 mJy beam^{-1}. Gaume and Mutel did detect some weak northern emission; they detected emission of 0.3 Jy beam^{-1} from two LCP spots just 5 mas apart (although their resolution gives them position errors of ∼60 mas). They also detected the weak, south-eastern, highly blueshifted emission at an unchanged flux, and a central-eastern RCP maser at 0.1 Jy beam^{-1}, the only maser emission of theirs that

Table 3. Variation in intensity of the northern masers over recent years.

Year	RCP flux (Jy beam^{-1})	LCP flux (Jy beam^{-1})
1982	<0.6	<0.6
1987	<0.15	0.3
1993	2.7	<0.075
1996	11.3	3.5

was not detected in the present work. Like Norris et al., they did not detect any northern RCP maser emission.

Agreement with observations in 1993 December (M. D. Gray et al., unpublished work) is excellent. Again, emission from the southern conglomerate of masers is the brightest emission with a peak of 5.3 Jy beam^{-1}, but Gray et al. did detect the northern RCP maser with a brightness of 2.7 Jy beam^{-1}. This demonstrates the appearance of a new maser over 11 yr, as shown in Table 3.

2.7 Morphology, line shapes and polarization at 1612 MHz

The small number of 1612-MHz masers shows simple morphology, especially in the north. The northern masers are very small, with an average semimajor axis of 4.7 mas, while the southern masers have an average semimajor axis of 8.4 mas. The southern masers (excepting the highly blueshifted far south-east maser) share a common orientation too: they all have position angles in the range of 70–95°, with a mean of 79°. The rough line the masers make on the sky also has an angle of ∼80°. It could be that whatever is causing these masers to lie in a rough line is also responsible for position angles; possibly they line up with a weak advanced shock off the southern edge of the UCH II region.

The 1612-MHz maser line shapes are, in general, very well approximated by Gaussians. The average FWHM of the 1612-MHz masers which were fit with a Gaussian is ∼275 m s^{-1}, which is in good agreement with the figure of ∼280 for 1665 MHz (see Table 1).

This is the first VLBI data set of 1612 MHz in W3(OH) which contains all polarization data. All of the masers are highly circularly polarized. For the most intense masers, the circular polarization is very close to 100 per cent, with negligible linear and unpolarized emission. The only masers to have less than 90 per cent circular polarization have low fluxes, and are subject to larger errors. The only maser to have significant linear polarization is interesting – it is the highly blueshifted maser in the extreme south-east of the map. This linear polarization correlates with the much more numerous 1665-MHz data (see Section 3.3). Even as a single feature, it is clear that this maser is not associated with the main southern group.

2.8 Magnetic field and velocity structure at 1612 MHz

Six Zeeman pairs were found – the first to be found in 1612 MHz inW3(OH). They are shown in Table 4. With only three of the masers not in a Zeeman pair, this means that 80 per cent of the masers were paired. All the masers not in Zeeman pairs were in the southern group and, from the map, all of them were spatially isolated. It is not possible to say whether their solitary nature is responsible for the lack of a Zeeman partner; because they are weak masers, the chance of observing an even weaker partner is slim.

The median ratio of the fluxes of the Zeeman pairs is 3.7 : 1, and the mean is 3.5 : 1. At 1612 MHz, there are three possible Zeeman pair separations that can theoretically result from the same magnetic field strength. A full pattern has never been seen; only one pair of lines has ever been observed. The question is then: which pair is being observed? It might be expected that the Zeeman pair which results from the intrinsically strongest σ transitions is the one being observed. On comparing the various magnetic field strengths possible in the satellite lines with unambiguous field strengths from, for example, 1665 MHz, one does indeed find the best agreement for this Zeeman pair. There remains the possibility that the observed Zeeman pairs could result from more than one pair of σ transitions. Fortunately, the second-strongest transitions have a splitting three times larger than the strongest pair. Therefore, ambiguity ought only to be a problem when unexpectedly large magnetic field strengths are encountered, such that a field strength of one-third as much is also reasonable. The highest magnetic field in Table 4 is 10.7 mG – alternative values are 3.5 and 2.1 mG – whilst the lowest field strength is 4.8 mG. It is not inconceivable therefore, but unlikely, that the 10.7-mG field is actually a wider Zeeman pair in a field of 3.5 mG.

The range of magnetic field strengths is ∼5 to ∼11 mG, which is in agreement with magnetic field measurements at 1665 MHz, and also with the previous 1612-MHz Zeeman pair measured in W49 by Gaume & Mutel (1987), which gave a field of 9.1 mG. Unfortunately, the blueshifted feature at −47.5 km s^{-1} does not have a Zeeman partner, so its unusual velocity cannot be probed further (but see Section 3.3 for comparisons with other ground-state masers in the vicinity).

2.9 1720-MHz masers

Fig. 7 shows the Stokes *I* spectrum of the maser fluxes calculated from the channel maps. The 1720-MHz maser spot map is shown in Fig. 8. All the 1720-MHz emission is concentrated in three very small areas of emission– in the north, south and west – making it the simplest of all the ground-state OH lines.

W3(OH) was observed at 1720 MHz by Lo et al. (1975), who deduced, using early VLBI, that the LCP/RCP doublet at that

Table 4. 1612-MHz Zeeman pairs (assuming smallest magnetic splitting). Information for peak flux, RA and Dec. are from the peak channel in the brighter of the two Zeeman components.

Peak flux density (Jy beam^{-1})	RA offset (mas)	Dec. offset (mas)	Magnetic field (mG)	Magnetic field error ±(mG)	Demagnetized velocity (km s^{-1})	Demagnetized velocity error ±(km s^{-1})	Pair quality	Location
11.34	−50.3	−214.2	7.56	0.39	−42.97	0.02	a	North
0.99	−38.7	−213.4	7.37	0.51	−43.19	0.03	a	North
0.78	9.3	−113.2	10.68	0.53	−42.39	0.03	b	North
1.97	172.6	−1817.7	8.41	0.54	−42.67	0.03	a	South
1.53	112.8	−1831.9	7.92	0.53	−43.42	0.03	a	South
1.15	195.6	−1816.4	4.65	0.54	−42.84	0.03	b	South

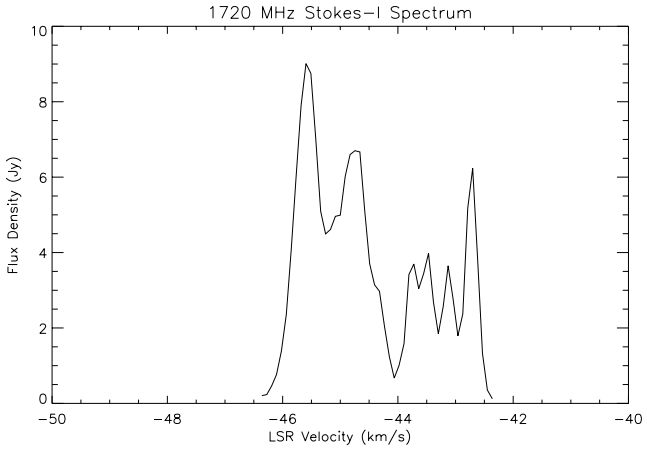

Figure 7. The Stokes *I* spectrum of the maser fluxes at 1720 MHz, calculated from the channel maps.

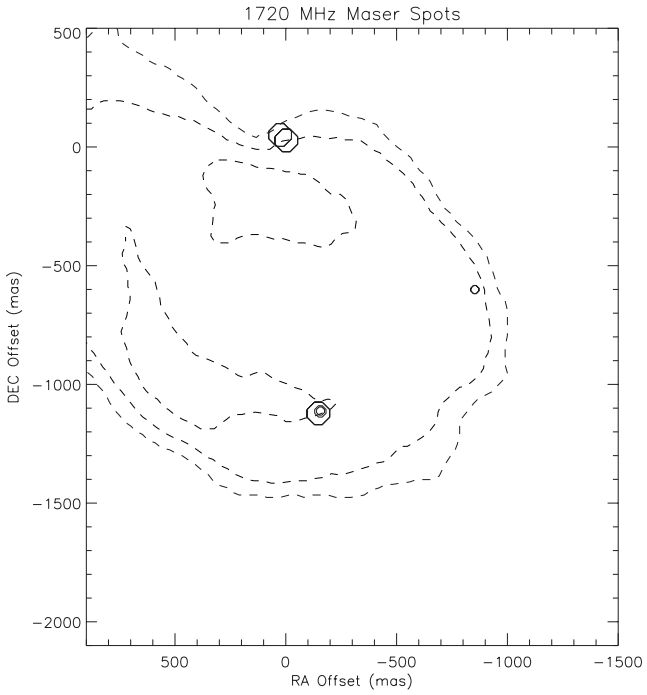

Figure 8. The 1720-MHz maser spot map. Contours are the 0.5, 7.1 and 16.6 mJy beam^{-1} levels of a VLA 2-cm continuum map (Masheder et al. 1994, and references therein). The spots are divided into three classes, represented by symbols of different sizes. In order of increasing symbol size, and maser flux, these classes are: (i) <0.4 Jy; (ii) 0.4–2.0 Jy; (iii) 2.0–10.0 Jy.

frequency was separated by less than 3 mas, providing some of the first strong evidence of the Zeeman effect in these masers. The next work was by Fouquet & Reid (1982), who published multifrequency ground-state observations of W3(OH). As was mentioned with respect to 1612 MHz, Fouquet and Reid suffered from very poor sensitivity in their observation, and they detected just one 1720-MHz maser. The position of this maser matches well with the brightest 1720-MHz maser in the present work, in the north of the map. Gaume & Mutel (1987) observed W3(OH) at 1720 MHz, along with the other ground-state lines, but were only able to observe in RCP at 1720 MHz. They detected five masers in two clusters, which lie roughly over the northern and southern emission shown in fig. 6.2-3 of that work. Before the present work, the best data at 1720 MHz came from the extremely high-resolution observation by Masheder et al. (1994). Masheder et al. observed for 12 h in LCP in 1989 November with two antennas in the US, one in China, one in Sweden, and the 100-m antenna in Germany. This gave them long baselines giving a beam size of 2.4 mas and a 1σ noise of $\sim$24 mJy beam^{-1} – a higher resolution but lower sensitivity than the current data, and in only LCP. They also detected only the northern and southern emission; just one maser was found in the south and probably three masers in the north within about 15 mas (beam artefacts in their maps give some level of ambiguity to the identifications). The three masers in their northern area are so close that they are not individually resolved in the current data; all three are incorporated into the most intense feature.

Just 35 mas to the north-east, however, is a maser which was not detected by Masheder et al. (1994), and which in LCP has a flux density of 2.76 Jy beam^{-1} – and so clearly would have been detected if present in 1989. This is therefore a new maser, which has grown in the 7 yr between the epochs. In their fig. 4, Masheder et al. (1994) show that the 1720-MHz masers have been evolving slowly, in particular a feature has been intensifying at a velocity of about -45.5 km s^{-1} (LCP) over the last three decades. This velocity corresponds to the currently most intense maser.

The detection of the western source adds evidence to the alignment of 1720-MHz emission and 4765-MHz emission as suggested by Baudry et al. (1988), Baudry & Diamond (1991), Gray et al. (1992) and Masheder et al. (1994). More recent comparisons between 1720 and 4765 MHz clarify the association between the two frequencies (McLeod 1997; Gray et al. 2001; Palmer, Goss & Devine 2003).

W3(OH) has also been observed at 1720 MHz with MERLIN in 1993 December (Gray et al. 2001), in an attempt to detect co-propagation with the 4765-MHz line. With the much lower resolution of MERLIN (130 mas), the results agree very well in terms of maser positions and velocities with the current data. Co-propagation of 1720- and 4765-MHz masers has recently been confirmed at VLBA resolution by Palmer et al. (2003). The two close southern masers were not resolved in the MERLIN data, but the extra northern maser, not detected in Masheder et al. (1994), was detected. Fluxes, as determined by Gaussian fitting, were typically two to three times higher in the MERLIN data, suggesting that the 1720-MHz masers may be surrounded by slightly diffuse emission that is resolved out on longer baselines. The exception here is the northern maser that was not detected by Masheder et al. (1994), which has approximately the same flux in both more recent observations. There are two possible explanations for this: the maser does indeed have extended emission associated with it, but has been rapidly intensifying such that the core emission in the current data is roughly equal to the total emission in the earlier MERLIN data; or the maser has no extended emission, which may be related to its very recent appearance.

2.10 Morphology, line shapes and polarization at 1720 MHz

The three groups of masers are distinct morphologically. The northern masers are the smallest and most circular, having an average major axis of 4.6 mas. The southern masers are slightly larger, having an average major axis of 7.6 mas, while the western masers are much more elongated and well resolved, having an average major axis of 22.7 mas and a north–south position angle. It should be noted though that both northern and southern masers were unresolved in these observations, and so circular morphology would be expected; in the higher resolution observations of Masheder et al. (1994) they

Table 5. 1720-MHz Zeeman pairs (assuming smallest magnetic splitting). Information for peak flux, RA and Dec. are from the peak channel in the brighter of the two Zeeman components.

Peak flux density (Jy beam^{-1})	RA offset (mas)	Dec. offset (mas)	Magnetic field (mG)	Magnetic field error ±(mG)	Demagnetized velocity (km s^{-1})	Demagnetized velocity error ±(km s^{-1})	Pair quality	Location
7.13	−2.4	27.5	7.47	0.51	−45.17	0.03	a	North
5.08	25.8	50.6	6.80	0.41	−43.10	0.02	a	North
2.26	−147.0	−1122.1	5.70	0.46	−43.44	0.03	a	South
0.40	−156.0	−1113.7	6.02	0.51	−43.72	0.03	b	South
0.12	−853.0	−600.2	4.51	0.51	−44.91	0.03	b	East

were also unresolved, with a maximum size of 1.2 mas. The size of the western masers suggests that they are more diffuse than the others, which would explain why the flux measured by MERLIN is so much higher. It is likely that the 1720-MHz masers consist of a bright core containing ∼50 per cent of the flux in <1.5 mas, and an extended halo (>10 mas) containing the remaining 50 per cent of the flux.

Of the masers with enough channels for Gaussian fitting, all except the most intense maser were well fitted. The maser that failed did so because of a shoulder on the emission; this shoulder is possibly the underlying unresolved maser that was resolved in Masheder et al. (1994). If a second Gaussian is fitted, it is possible to obtain an additional feature of peak brightness equal to 2 Jy beam^{-1} with a central velocity of −44.3 km s^{-1}. However, this most intense 1720-MHz feature is spatially very close to the peculiar feature number 64, at 1665 MHz, and separated from it by only 1 km s^{-1} in velocity (see Paper I, Section 3.3). The shoulder could therefore also result from a velocity gradient effect, perhaps involving a collision, as suggested for the 1665-MHz line shape. We note that the shoulder on the 1720-MHz feature is on the opposite side of the line profile from that on feature 64 at 1665 MHz. The mean FWHM of the 1720-MHz masers which were fitted with Gaussians is ∼299 m s^{-1}, which is in fair agreement with the figure of ∼280 m s^{-1} for 1665 MHz. It should be noted that the FWHM of the most intense maser is 509 m s^{-1}, which is one of the highest FWHM of any maser in the ground state. This is possibly because of the unresolved multiple nature of this maser. Without this maser, the mean FWHM is ∼257 m s^{-1} (Table 1).

This is the first VLBI data set of 1720 MHz in W3(OH) that contains all polarization data. All of the masers are highly circularly polarized; no maser has less than 90 per cent total or circular polarization. For the brightest masers, the circular polarization is very close to 100 per cent, with negligible linear and unpolarized emission. Only the western masers, which are both very weak and therefore subject to larger polarization errors, have any detectable linear polarization. This means that the 1720-MHz masers show the least deviation from total circular polarization of any line in the ground state.

2.11 Magnetic field and velocity structure at 1720 MHz

Five Zeeman pairs were found, comprising all of the masers detected. From single-dish spectra, it was clear that the 1720-MHz emission exhibits a relatively clear Zeeman pattern, and this is reflected in the above result. The Zeeman pairs are shown in Table 5. Magnetic field measurements are in good agreement with Gray et al. (2001).

The median ratio of the fluxes of the Zeeman pairs is 1.4 : 1, and the mean is 1.8 : 1. This represents the most balanced Zeeman pairing amongst the ground-state lines – the conditions in which

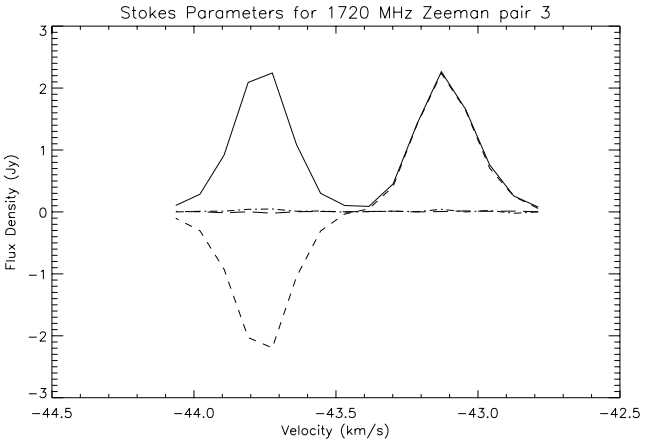

Figure 9. The most perfect Zeeman pair in W3(OH), at 1720 MHz. The Stokes parameters in this, and every subsequent, diagram are determined by the following line styles: solid – I; long-dashed – Q; dot-dashed – U; short-dashed – V.

1720-MHz masers form are clearly also favourable for near-perfect Zeeman patterns. The Zeeman pair at offsets ∼(147, 1122) is the most perfect Zeeman pair detected in the whole data set; the peak fluxes balance to within 1 per cent. Its Stokes lineshape is shown in Fig. 9.

As with 1612 MHz, there are three possibilities for the magnetic field strength required to produce a certain splitting because three separate pairs of σ transitions can theoretically be involved. However, only one pair of lines is ever observed at 1720 MHz. It is therefore most likely that, as with 1612 MHz, all the masers observed are formed in the intrinsically strongest pair of transitions. Using this assumption, the range of the magnetic field strengths is ∼4.5 to ∼7.5 mG, which is in good agreement with the masers at the other ground-state frequencies, and with Lo et al. (1975) who measured a field of 6 mG at 1720 MHz.

3 COMPARISONS BETWEEN THEGROUND-STATE LINES

3.1 Co-propagating masers

The complete mapping of the four ground-state lines in W3(OH) allows, for the first time, searches for co-propagating masers from different lines at VLBI resolution, and alignment of images at different ground-state frequencies with an accuracy of ∼1 mas. Such an alignment is shown in Fig. 10. It has long been known that many of the masers at 1612, 1667 and 1720 MHz lie near or amongst 1665-MHz masers (Fouquet & Reid 1982). In the present data, only two 1612-MHz masers, three 1667-MHz masers and no 1720-MHz

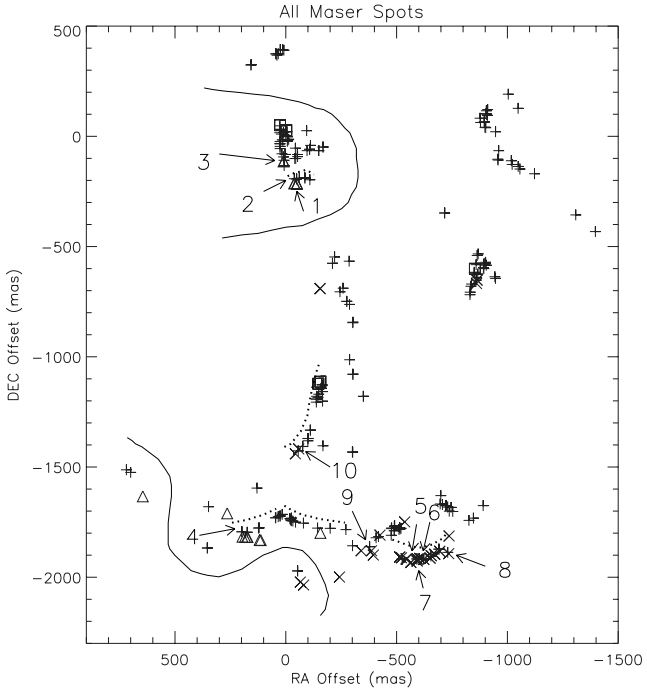

Figure 10. The ground-state masers in W3(OH). Regions of distinct velocity profile are bounded by the thin solid lines. Dashed lines indicate strings of masers that may outline shocks. Overlaps are referred to in the text by number. Maser frequencies are indicated by the following symbols: plus signs, 1665 MHz; crosses, 1667 MHz; triangles, 1612 MHz; squares, 1720 MHz.

masers lie 100 mas or more from a 1665-MHz maser. No other masers lie more than 200 mas from a 1665-MHz maser. These figures are exactly what is expected from the two-point correlation analysis, performed in Paper I. We note that the two-point correlation function begins to rise steeply for separations smaller than 250–300 mas. Clearly, the lines other than 1665 MHz are not exceptional in this respect.

This information will be of importance in observations at lower resolutions when looking for coincident masers at other frequencies or in other sources. Immediately striking is the number of closely coincident masers of 1665 and 1667 MHz in the south-west at the location of the arc feature, which will be examined in detail. Also notable is the lack of masers from any frequency other than 1665 MHz in the north-west and far north-east of W3(OH) (1665-MHz maser groups *a* and *b*).

The much larger number of 1665-MHz masers means that even in unrelated random distributions we would expect to see the most spatial coincidences between 1665-MHz masers and those of other frequencies, and this is indeed seen. The criterion for masers to be considered coincident is important here. Given the accuracy of alignment of the maps, and the criterion applied when considering coincident masers for Zeeman pair candidature (12 mas), it was decided that the same criterion would be applied to the different frequencies, with separations of 0–6 mas having the highest confidence. In addition, coincident masers with separations 12–24 mas would be examined with caution.

Maser coincidences and an assessment of the likelihood of co-propagation are shown in Table 6. The masers were checked for agreement within the error of their demagnetized velocity and magnetic field strengths. Where there was only one maser at one frequency and a Zeeman pair at the other frequency, the velocity of the maser was used under the assumption that its demagnetized velocity was equal to that of the Zeeman pair at the other frequency. From this, the magnetic field that would be required to give the correct Zeeman splitting was calculated, and compared to that of the Zeeman pair. Where there is only one maser at either frequency, a magnetic field can always be found which will give the required separation – the test then becomes whether this magnetic field is in agreement with other Zeeman pairs in the area. Clearly, this test is less rigorous than direct comparison of demagnetized velocities and field strengths. The overlaps are categorized into classes A, B, C and D, where A is probable co-propagation, B is possible association, C is indeterminate, and D is probably not co-propagation.

There are no three-frequency or four-frequency overlaps, not even at 25-mas separation (∼50 au). All overlaps are between 1665 MHz and one other ground-state frequency. This will be a useful constraint to future modelling of star-forming region masers.

There are no instances of co-propagation between 1720 and 1665 MHz above the detection threshold of 75 mJy, so previous map alignments of strong sources at these frequencies by other authors are therefore invalid. However, all 1720-MHz emission comes from regions with significant and numerous 1665-MHz masers, and it is likely that the activity at both frequencies has a common cause.

There is just one class A overlap between 1612 and 1665 MHz, labelled 3 in Fig. 10. The magnetic fields derived from the two frequencies differ by 0.59 mG, but the uncertainty in the field at 1612 MHz is 0.53 mG. Also of interest are the class B overlaps labelled 1, 2 and 4. From Fig. 10 it can be seen that 1612-MHz masers lie ∼20 mas from lines or 'chains' of 1665-MHz masers of the same demagnetized velocity and magnetic field strength. The 1612-MHz masers could be in the same body of gas as the 1665-MHz masers, but separated by ∼40 au. If the chains of 1665-MHz masers delineate shocks in the gas, then the 1612-MHz masers probably just precede or just trail the 1665-MHz emission in the shocks. In the north, in 1665-MHz maser region *c*, the direction of any shock is unclear, but in the south, in maser group *f* (overlap 4), any shock would most likely be propagating to the south. In this case, the 1612-MHz masers lie physically ahead of the 1665-MHz masers in the shock, at an earlier stage in the shocking process. Applying this to the northern overlaps, this suggests that the shocks are also propagating south from the centre of maser group *c*. We justify the identification of the chains of masers with shocks, because masers in the chains have spots which are elongated along the axis of the local chain.

The remaining six class A and B overlaps are all between 1665 and 1667 MHz. The largest number of overlaps is expected between these two frequencies because they have the most numerous maser spots. The two class B overlaps, 8 and 9, are classed as such because each consists of a single Zeeman component from each frequency. This means that a single velocity and magnetic field can always be calculated for the two masers. Overlap 10 has a calculated magnetic field value outside the error range, and is therefore classed as B. From Fig. 10, it is clear that the arc feature in the south of W3(OH) is the source of several good overlaps. Fig. 11 shows contour maps of the arc feature in both 1667 and 1665 MHz, where it is also visible.

While all the 1665- and 1667-MHz masers in the arc feature have similar magnetic field and velocity values – and are therefore almost certainly in the same body of gas – only those in the centre of the arc (between RA offsets −580 and −630) have the same magnetic field and velocity values, and can therefore be justified as co-propagating. The excellent positional agreement between the co-propagating masers, and indeed the positional agreement in each Zeeman pair, is testimony to the high accuracy of alignment between the maser maps. There are also three class C overlaps in the arc

Table 6. Maser overlaps among the ground-state lines. Overlaps between frequencies are classed A to D on agreement in demagnetized velocity and magnetic field strength between the frequencies.

Transition frequency (MHz)	Integrated feature flux (Jy)	Peak flux density (Jy beam^{-1})	RA offset (mas)	Dec. offset (mas)	V_{LSR} (km s^{-1})	Circular direction	Zeeman pair number	Magnetic field (mG)	Magnetic field error ±(mG)	Demagnetized velocity (km s^{-1})	Demagnetized velocity error ±(km s^{-1})	Overlap separation (mas)	Calculated field (mG)	Overlap class
1612	11.54	3.53	−50.3	−214.2	−43.46	L	1	7.82	0.39	−42.97	0.02			
1612	42.12	11.34	−50.3	−214.2	−42.55	R	1	7.82	0.39	−42.97	0.02	21.0		B
1665	7.88	1.78	−48.9	−193.2	−40.69	R	22	7.58	0.09	−42.93	0.03			
1665	121.56	27.03	−48.6	−193.1	−45.18	L	22	7.58	0.09	−42.93	0.03			
1612	2.66	0.98	−38.7	−213.5	−42.73	R	2	7.63	0.51	−43.19	0.03			
1612	2.91	0.99	−38.7	−213.4	−43.64	L	2	7.63	0.51	−43.19	0.03	21.0		B
1665	0.73	0.33	−38.2	−192.4	−45.44	L	–	–	–	–	–		7.61	
1612	0.42	0.19	9.7	−113.7	−41.73	R	6	11.06	0.53	−42.39	0.03			
1612	2.60	0.78	9.3	−113.2	−43.00	L	6	11.06	0.53	−42.39	0.03	4.6		A
1665	7.70	2.09	8.2	−108.8	−45.53	L	–	–	–	–	–		10.65	
1612	2.02	0.36	175.0	−1818.0	−43.18	L	4	8.71	0.54	−42.67	0.03			
1612	13.87	1.97	172.6	−1817.7	−42.09	R	4	8.71	0.54	−42.67	0.03	21.9		D
1665	1.23	0.30	174.2	−1795.9	−43.77	L	–	–	–	–	–		3.74	
1612	5.28	0.51	184.0	−1817.2	−43.09	L	5	4.81	0.54	−42.84	0.03			
1612	8.67	1.15	195.6	−1816.4	−42.64	R	5	4.81	0.54	−42.84	0.03	22.6		B
1665	2.27	0.73	198.1	−1793.9	−41.57	R	52	4.78	0.09	−43.00	0.03			
1665	20.35	4.66	198.5	−1793.5	−44.38	L	52	4.78	0.09	−43.00	0.03			
1665	1.09	0.25	−690.5	−1872.4	−44.82	L	54	6.29	0.10	−42.98	0.03			
1665	64.06	10.08	−691.3	−1872.7	−41.13	R	54	6.29	0.10	−42.98	0.03	10.2		C
1667	9.23	1.98	−694.5	−1882.4	−42.28	R	3	6.58	0.17	−43.42	0.03			
1667	6.50	1.18	−695.1	−1882.6	−44.65	L	3	6.58	0.17	−43.42	0.03			
1665	49.62	10.94	−591.4	−1916.9	−45.53	L	55	6.69	0.08	−43.52	0.02			
1665	32.83	7.12	−591.6	−1916.9	−41.57	R	55	6.69	0.08	−43.52	0.02			
1667	13.14	3.69	−592.8	−1917.7	−44.82	L	12	6.57	0.14	−43.63	0.02	1.2		A
1667	5.93	1.37	−594.0	−1917.7	−42.45	R	12	6.57	0.14	−43.63	0.02			
1665	0.67	0.29	−621.9	−1917.9	−45.44	L	56	6.87	0.11	−43.41	0.03			
1665	1.87	0.49	−622.0	−1918.0	−41.40	R	56	6.87	0.11	−43.41	0.03	1.0		A
1667	3.71	0.74	−622.4	−1918.9	−44.65	L	10	6.77	0.16	−43.43	0.03			
1667	1.77	0.34	−623.4	−1919.4	−42.28	R	10	6.77	0.16	−43.43	0.03			
1665	0.91	0.28	−654.8	−1903.9	−41.31	R	–	–	–	–	–	2.5	7.60	C
1667	4.59	1.55	−656.8	−1902.4	−42.10	R	5	6.59	0.17	−43.25	0.03			
1667	3.99	1.35	−656.8	−1902.5	−44.39	L	5	6.59	0.17	−43.25	0.03			
1665	1.57	0.29	−526.5	−1919.0	−41.22	R	57	6.90	0.11	−43.30	0.03			
1665	2.56	0.56	−525.0	−1916.3	−45.35	L	57	6.90	0.11	−43.30	0.03	5.5	5.74	C
1667	0.99	0.33	−522.1	−1911.6	−42.28	R	–	–	–	–	–			
1665	3.42	1.16	−601.5	−1915.0	−45.53	L	–	–	–	–	–	2.4	6.30	A

Table 6 – *continued*

Transition frequency (MHz)	Integrated feature flux (Jy)	Peak flux density (Jy beam^{-1})	RA offset (mas)	Dec. offset (mas)	V_{LSR} (km s^{-1})	Circular direction	Zeeman pair number	Magnetic field (mG)	Magnetic field error ±(mG)	Demagnetized velocity (km s^{-1})	Demagnetized velocity error ±(km s^{-1})	Overlap separation (mas)	Calculated field (mG)	Overlap class
1667	11.55	2.02	−603.9	−1914.9	−44.82	L	11	6.36	0.17	−43.67	0.03			
1667	1.35	0.38	−604.3	−1914.9	−42.54	R	11	6.36	0.17	−43.67	0.03			
1665	0.59	0.22	−730.7	−1887.2	−44.56	L	–	–	–	–	–	7.4	7.44	B
1667	0.75	0.16	−735.3	−1893.0	−43.68	L	–	–	–	–	–			
1665	14.67	2.58	−418.3	−1815.5	−44.47	L	–	–	–	–	–	9.4	∼0	D
1667	2.15	0.59	−425.1	−1809.0	−44.03	R	–	–	–	–	–			
1665	2.65	0.78	−378.4	−1861.6	−44.74	L	–	–	–	–	–	19.9	4.46	B
1667	87.32	9.29	−386.7	−1879.7	−44.21	L	–	–	–	–	–			
1665	1.46	0.74	−56.0	−1426.5	−44.91	L	–	–	–	–	–	7.9		B
1667	0.48	0.09	−60.9	−1420.4	−44.30	L	13	4.22	0.18	−43.55	0.03		4.61	
1667	1.23	0.26	−58.6	−1418.1	−42.81	R	13	4.22	0.18	−43.55	0.03			
1665	3.06	0.71	−861.3	−642.1	−46.05	L	30	3.19	0.09	−45.11	0.03			
1665	71.20	6.40	−859.1	−652.2	−44.21	R	30	3.19	0.09	−45.11	0.03	3.4		C
1667	1.54	0.18	−862.5	−651.7	−45.53	L	1	2.43	0.18	−45.10	0.03			
1667	3.29	0.41	−863.8	−652.5	−44.65	R	1	2.43	0.18	−45.10	0.03			
1665	2.95	0.60	−838.0	−670.1	−43.95	R	–	–	–	–	–	22.7	5.93	D
1667	1.25	0.37	−860.6	−667.5	−44.65	R	–	–	–	–	–			
1665	3.02	0.91	26.8	47.6	−41.48	R	–	–	–	–	–	2.9	5.48	C
1720	10.49	2.76	25.7	50.3	−43.47	L	2	6.57	0.41	−43.10	0.02			
1720	19.73	5.08	25.8	50.6	−42.70	R	2	6.57	0.41	−43.10	0.02			
1665	1.47	0.34	−164.5	−1128.5	−45.79	L	34	4.89	0.11	−44.33	0.03			
1665	12.93	2.46	−162.7	−1126.0	−42.89	R	34	4.89	0.11	−44.33	0.03			
1720	2.17	0.40	−156.0	−1113.7	−43.38	R	5	5.82	0.51	−43.72	0.03	14.0		D
1720	0.31	0.11	−156.6	−1112.3	−44.06	L	5	6.02	0.53	−43.72	0.03			
1720	11.47	2.24	−147.0	−1122.2	−43.72	L	3	5.51	0.46	−43.44	0.03	16.2		D
1720	11.01	2.26	−147.0	−1122.1	−43.13	R	3	5.70	0.47	−43.44	0.03			
1665	4.80	0.87	−4.6	20.9	−48.52	L	9	7.37	0.11	−46.29	0.03			
1665	88.59	15.54	−4.5	21.0	−44.03	R	9	7.37	0.11	−46.29	0.03	6.9		D
1720	60.67	7.13	−2.4	27.5	−45.60	L	1	7.21	0.51	−45.17	0.03			
1720	54.57	5.08	−2.4	27.7	−44.74	R	1	7.21	0.51	−45.17	0.03			
1665	0.93	0.15	−858.6	−582.0	−43.86	R	–	–	–	–	–	19.6	3.58	D
1665	13.98	2.74	−850.6	−616.8	−45.70	L	28	3.14	0.10	−44.80	0.03			
1665	11.05	2.05	−850.5	−619.5	−43.86	R	28	3.14	0.10	−44.80	0.03	18.8		D
1720	0.73	0.12	−853.3	−600.9	−44.66	R	4	4.36	0.51	−44.91	0.03			
1720	1.01	0.12	−853.0	−600.2	−45.17	L	4	4.36	0.51	−44.91	0.03			

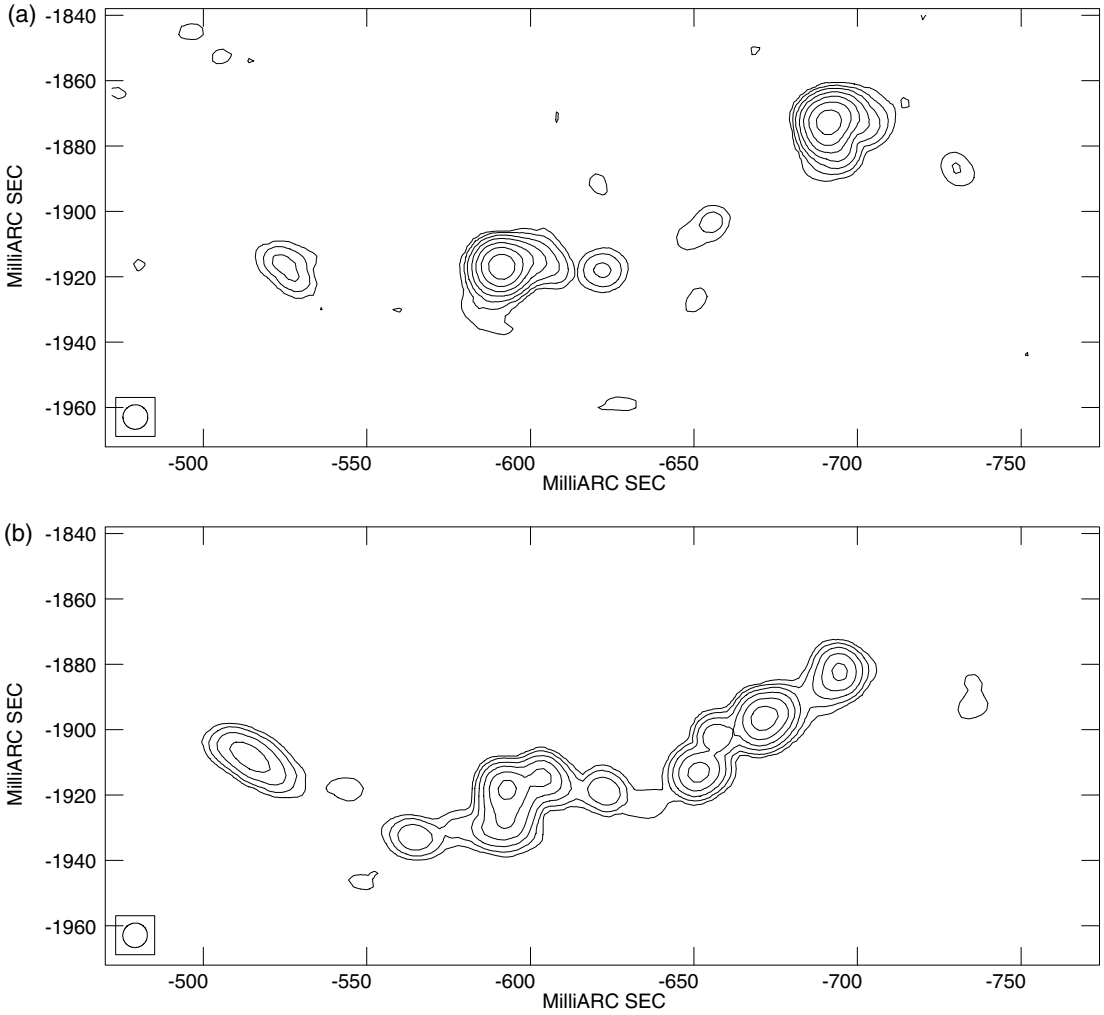

Figure 11. The southern arc feature in both (a) 1665-MHz and (b) 1667-MHz emission. The contours here indicate maximum channel intensity, not integrated intensity. Contours are at intervals of 100 mJy beam^{-1}.

features, and it is possible that the difficult nature of the Gaussian fitting in this complex area has resulted in the loss of some co-propagating masers. From Fig. 11 it appears that there could be co-propagation at ~ -690 mas where a strong 1665-MHz maser has swamped weaker maser emission a few mas to the west.

The integrated fluxes and integrated flux ratios of all class A and B overlaps are shown in Table 7. The integrated flux ratio is defined as the flux of the brighter line in the overlap, divided by the flux of the weaker; fluxes were calculated by totalling the Stokes *I* emission in the case of Zeeman pairs. Emission ratios such as these are extremely useful for comparison with results of maser models. In three of the four class A overlaps, the same hand of polarization is the stronger at both frequencies, which would be expected because both frequencies are experiencing the same velocity field, so we would expect all of the overlapping masers to exhibit this property. One possible reason why this does not happen in one case of apparent overlap is that it may not be a true overlap, but simply a coincidence of projection. In this case, the two observationally coincident masers could be experiencing velocity gradients in different directions, but additional coincidences of velocity and magnetic field strength lead us to suspect co-propagation.

The total integrated flux from all of the overlapping 1667-MHz masers is 127 Jy, while the total integrated flux from their 1665-MHz partners is 93 Jy. This slightly higher value for 1667 MHz is in stark contrast with the values for the W3(OH) area as a whole, where the total flux from 1665 MHz is about 15 times larger. This indicates that there is no justification in taking the ratios of emission at different frequencies from any large-scale region to be indicative of the true ratios resulting from co-propagation. In extragalactic megamasers, there is usually a $\sim 3:1$ excess of 1667-MHz emission for the source as a whole. Compact emission from megamasers is almost entirely at 1667 MHz (Lonsdale et al. 1998) so these extragalactic sources clearly favour 1667 MHz over 1665 MHz. However, there is no other obvious link between megamasers and co-propagating maser spots in Galactic star-forming regions. In the light of these results concerning the strength of masers co-propagating at 1665 and 1667 MHz, future observers looking for co-propagation should consider looking at maser spots where 1667 MHz is the dominant maser. It is also worth noting at this point that the work of Thissen et al. (1999) predicts 1667 MHz to be the dominant maser resulting from a pumping scheme which arises from photodissociation of OH. Criticisms of their chemical-pump model have centred on the lack of a replenishable source of OH, because each molecule can mase only once before dissociation. If the arc is indicative of a shock, then this is just the environment where locally produced ultraviolet (UV) radiation could produce large amounts of freshly

Table 7. The integrated fluxes of all class A and B overlaps. Ratios of the integrated fluxes are in the outer columns.

Ratio	Overlap 1 (B)	Flux left (Jy)	Flux right (Jy)	Overlap 5 (A)	Flux left (Jy)	Flux right (Jy)	Ratio
1	1612	11.54	42.12	1665	49.62	32.83	4.3
2.4	1665	121.56	7.88	1667	13.14	5.93	1
	2 (B)	Left	Right	6 (A)	Left	Right	
7.6	1612	2.91	2.66	1665	0.67	1.87	1
1	1665	0.73	–	1667	3.71	1.77	2.2
	3 (A)	Left	Right	7 (A)	Left	Right	
1	1612	2.60	0.42	1665	3.42	–	1
2.6	1665	7.70	–	1667	11.55	1.35	3.8
	4 (B)	Left	Right	8 (B)	Left	Right	
1	1612	5.28	8.67	1665	0.59	–	1
3.2	1665	20.35	2.27	1667	0.75	–	1.3
				9 (B)	Left	Right	
				1665	2.65	–	1
				1667	87.32	–	33.0
				10 (B)	Left	Right	
				1665	1.46	–	1
				1667	0.48	1.23	1.2

Table 8. Polarization and Zeeman pair properties of the ground-state OH maser lines. The 'Zeeman ratio' is the ratio of the intensity of the stronger peak to the weaker peak. The value marked with an asterisk has had two outliers dropped from the sample.

Frequency (MHz)	Number of masers	Integrated flux (Jy)	Zeeman pair (per cent)	Median Zeeman ratio	Mean Zeeman ratio	RCP (per cent)	LCP (per cent)
1612	15	107	80	3.7	3.5	53	47
1665	211	4250	55	4.4	6.9*	42	58
1667	40	276	68	1.7	2.1	46	54
1720	10	172	100	1.4	1.8	50	50

dissociated OH, and result in a transient burst of masing. As such, the arc may represent an environment where the dominant maser pump is chemical.

What is surprising is the very small number of co-propagation cases that arise. Using just the class A overlap for 1612 MHz and the A and B overlaps for 1667 MHz, we find detectable co-propagation in just 7 per cent of 1612-MHz masers, and 3 per cent of masers at 1665 MHz.

3.2 Polarization

All of the ground-state lines show the occurrence of Zeeman pairs. The occurrence rates of Zeeman pairs should constrain the development of theories that explain why Zeeman components are often suppressed. A comparison of the Zeeman properties of the four lines is shown in Table 8.

1665 MHz has the largest sample size and the largest deviation from equality in the number of masers of each hand of polarization. This makes a significance test valid for this frequency. If LCP masers are assumed equally likely as RCP masers, then the significance of this deviation (continuity corrected) is 2.34 standard deviations. The 'two-tailed' probability associated with values as extreme as this, or more extreme than this, in the normal distribution, is 0.0193. This deficit of RCP is unlikely therefore to be random, and is probably rooted in the physical conditions which cause the masing; the most likely candidate is the velocity shift present, and therefore this surplus of one hand could indicate a prevailing velocity shift over the region. A velocity gradient provides a symmetry-breaking mechanism which can affect both pumping and propagation of masers. One Zeeman component can be favoured in propagation by, for example, the Cook mechanism (Cook 1966) or by biases in the optical depths of pumping lines.

Fig. 12 shows the variation of 'Zeeman probability' (percentage of masers in a Zeeman pair, down to our detection limit for the fainter component of 75 mJy) at each frequency with the Zeeman component splitting at that frequency; the component splitting is related to the Landé factor for the transition. As suggested in section 3.5 of Paper I, this appears to have major implications for theories

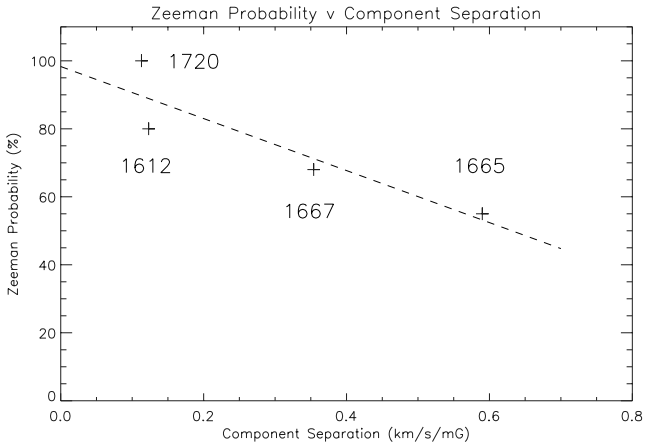

Figure 12. Variation of Zeeman probability with Zeeman component splitting at the four ground-state frequencies.

that explain how Zeeman pairs are destroyed, such as that of Nedoluha & Watson (1990). Nedoluha & Watson suggested that single Zeeman components would tend to be formed in areas of low magnetic field, while Fig. 12 suggests the opposite. A note of caution here: it is not possible to calculate the magnetic field of single Zeeman components, so it is not possible to know whether these singlets sample a particular range of magnetic fields. Therefore, there is no way of knowing whether masers at, for example, 1667 MHz would show the same Zeeman probability as those at 1665 MHz if they were in a magnetic field that was, on average, 66 per cent stronger (which would give both frequencies the same average Zeeman splitting). Clearly, this raises difficult questions of the theory of Nedoluha & Watson, and may require that the earlier theory by Cook (1966) be reinvestigated. Cook noted that a mechanism that introduces some asymmetry into the two σ transitions (and thereby favours one component over the other) could be obtained by appropriately matching the gradients of the magnetic field and velocity within the masing region. This does not appear to be contradicted by Fig. 12.

The Zeeman ratio also follows the general trend that the ratio is higher for larger Landé factors, but not with such clarity as shown in Fig. 12. It is likely that the small sample size of 1612- and 1720-MHz masers affects this. The Zeeman ratio is likely to be an indicator of the effectiveness of the Zeeman overlap in the same way as the Zeeman probability. It is certain that larger Zeeman component separation leads to fewer Zeeman pairs. This is unfortunate because 1665 MHz is the most common maser and has the largest component separation, and so gives relatively the least magnetic field information. Observations at 6 and 13 GHz can give much more favourable results where magnetic field strengths or demagnetized velocities are concerned.

We use our full set of Zeeman pairs, at all the ground-state frequencies, augmented with excited-state data at 6 GHz (Desmurs et al. 1998) and 13 GHz (Baudry & Diamond 1998), to compile a contour map of the magnetic field in W3(OH). This contour map is shown in Fig. 13. The salient features of the map are a general weakening of the field with RA to the west of the map, and a region of significantly stronger field in the north-east. This region of stronger field underlies the maser group *c*, which is also peculiar in other respects (see Section 3.6 of Paper I).

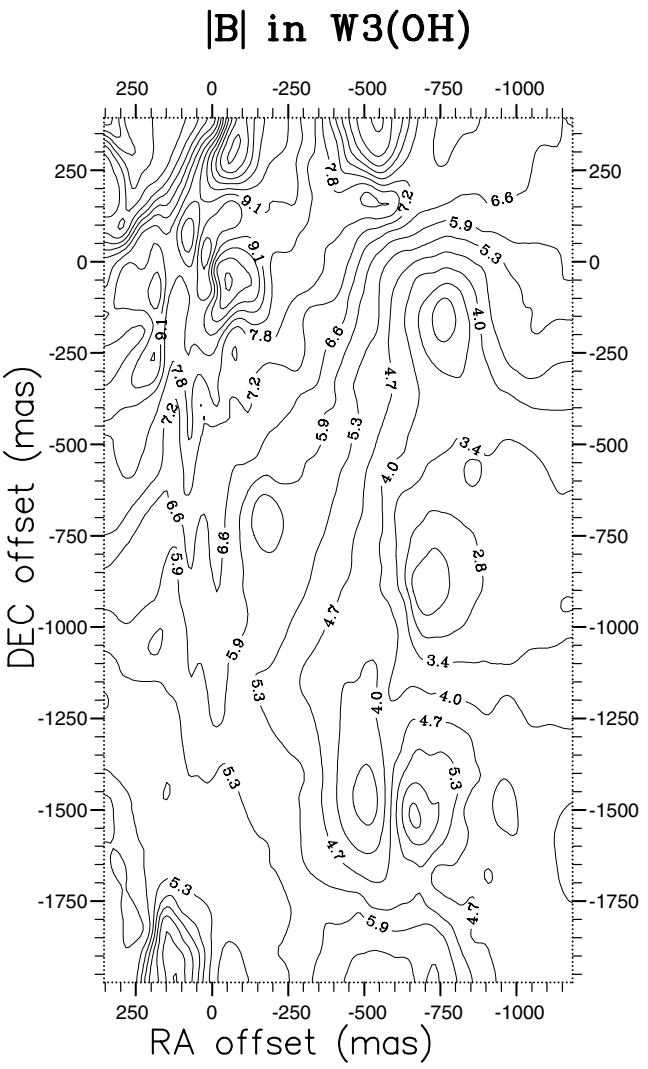

Figure 13. A contour map of the magnetic field in W3(OH) derived from Zeeman pairs from all four ground-state lines of OH, the 6-GHz excited lines (Desmurs et al. 1998) and the13-GHz lines (Baudry & Diamond 1998). Numbers on the contours indicate magnetic field strength in mG. The peak field strength in the map, near (0,0), is 12.3 mG. The edges of the map are fixed by the most extreme coordinate values for Zeeman pairs; we have no magnetic field information, derived from masers, outside the region shown. This contour map is based on a total of 211 points.

3.3 Velocity structure and magnetic field

The demagnetized velocity and magnetic field strengths of all the ground-state lines are shown in Fig. 14. All of the Zeeman pairs lie in the velocity range covered by 1665-MHz masers. All of the northern 1612-MHz masers appear to be in the same body of gas as 1665 maser group *c* (group *c* is highlighted by its large range of velocities and high magnetic field strengths); as do at least one and possibly both of the northern 1720-MHz masers. The rest of the 1612-MHz,1720-MHz, and all of the 1667-MHz masers lie within the velocity gradient delineated by the 1665-MHz masers, and therefore they probably share the motion of this gas. In Section 3.6 of Paper I, we argue that this motion is rotational with an expansion component. This picture is supported by the magnetic field values too. In both 1667 and 1720 MHz there are low field strengths in the area of 1665-MHz maser group *d*. In the south, two of the 1612-MHz masers have field strengths slightly greater than those of their 1665-MHz neighbours.

Fig. 15 shows the raw velocity data for all four lines without demagnetization. Most notable is that without demagnetization, the distribution of points looks like a scatter plot. As demonstrated in both Paper I and here (Paper II), demagnetization is essential to understanding the velocity structure of the source. Also notable are the small batch of masers that are very blueshifted at the south of the map, between about −1500 and −2000 mas offsets. The masers in this group are in the extreme south-east and extreme south of the map, except the right most of this group (arrowed in Fig. 15), which is nearer the centre of the map and is not associated with the rest. The remaining seven masers are all therefore on the fringes of the W3(OH) region, and do not share the velocity profile of either maser group *c* or the large-scale rotation. In the 1665-MHz masers in this area, there is evidence that the field may have swapped direction and so be pointing towards the observer. This could indicate that these masers lie just on the far side of W3(OH) because, this far from the centre of the UCH II region, the gas between us and the masers might not be sufficiently optically thick to shield these objects from

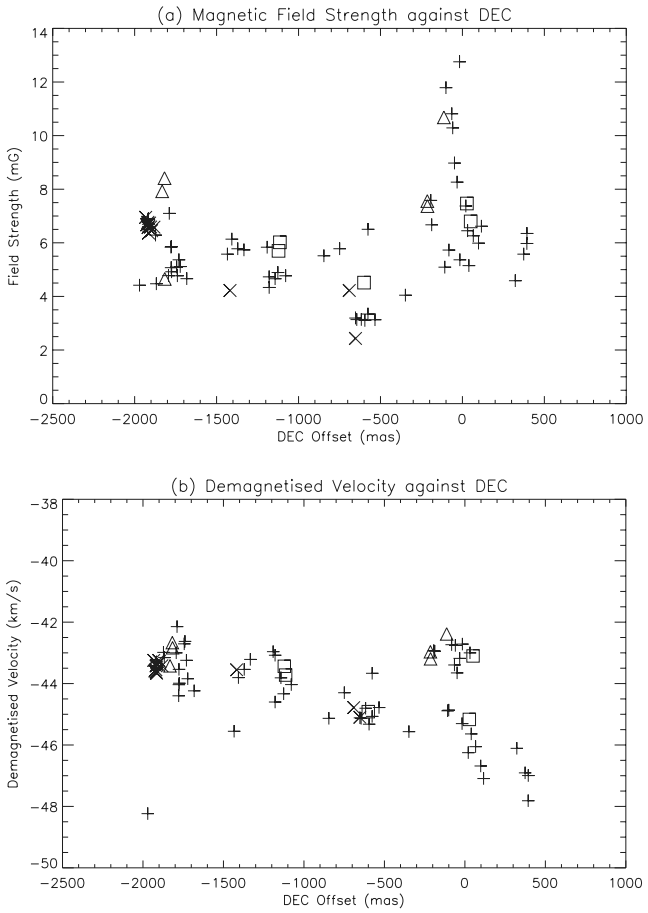

Figure 14. The magnetic field strength (a) and demagnetizedvelocity (b) plotted as functions of declination. Symbols denote the frequency (plus signs for 1665 MHz, crosses for 1667 MHz, squares for 1720 MHz and triangles for 1612 MHz).

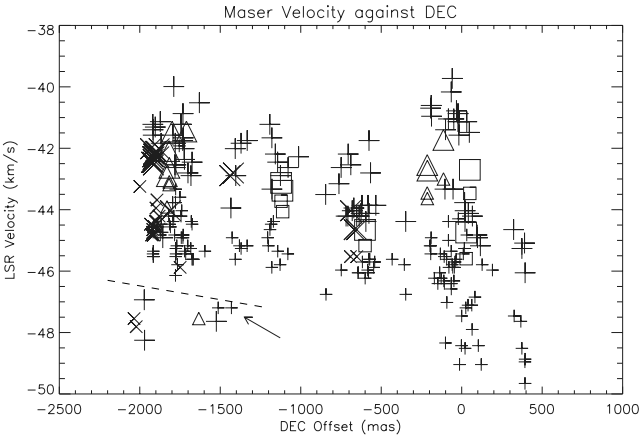

Figure 15. Raw, i.e. not demagnetized, velocities of all OHmasers in W3(OH). Symbols denote frequency (see Fig. 14) and polarization (large symbols are right circularly polarized; small symbols left).

view. In any case, these seven masers lie in a third distinct body of gas in the W3(OH) region.

3.4 Morphology

In general, the ground-state lines do not show different morphology at the individual maser level. 1612, 1665 and 1667 MHz all show lines or arcs of emission. 1720-MHz emission may be limited in its features by the small sample size, although 1720-MHz masers may be significantly smaller than the other frequencies, as shown by Masheder et al. (1994). In the west of the W3(OH) region, 1665-, 1667- and 1720-MHz masers in the vicinity of 1665-MHz maser group *d* all show elongated, resolved north–south geometry. This region is unique because it is the only place where masers of three transitions lie close to each other. The 1665-, 1667- and 1720-MHz masers lie within 50 mas (∼100 au) of each other, and are almost certainly in the same body of gas. Maser region *d* is typified by the lowest magnetic field strengths at all three frequencies. The extended nature of the masers in this region is a consequence of the lower field strengths, and therefore the lessened effect of magnetic beaming. The north–south geometry of the masers probably reflects real physical condensations in the gas.

4 CONCLUSIONS

The conclusions presented here are complementary to those in Paper I which dealt with the 1665-MHz masers. A complete catalogue of the data at all four frequencies and in all four Stokes parameters can be found on the Internet at http://www.star.bris.ac.uk/mark/w3oh.html. Further information can be found in Wright (2001).

From the general splitting of the LCP and RCP emission, it is clear that the magnetic field generally points away from the observer. Only in the far south-east is there evidence that the field may be reversed. The polarization of the masers shows a clear trend; the further from the centre of the W3(OH) region the masers are, the more linear polarization and unpolarized emission they exhibit and the less circular and total polarization they contain. This is interpreted as indicating a general change in orientation of the ambient magnetic field, such that moving north or south of the centre results in an increase of the angle between the magnetic field axis and the line of sight. This description might indicate that the magnetic field lines point towards the central star. It is tempting to suggest that the field lines in the disc lie radially, but given the differential rotation in a disc the lines would quickly wind up into a tight spiral. What is more likely is that with the 10° inclination of the disc we are seeing the field entering the disc from 'above' or 'below'.

Interpreting coincident RCP and LCP maser components as Zeeman pairs not only clarifies the otherwise messy velocity distribution of the masers, but also gives valuable information about the magnetic field strengths. The magnetic field strength is found to be fairly constant within each maser cluster, with typical values of ∼5–7 mG. The exception is maser group *c*, which exhibits a wide range of magnetic field strengths from 5 to 13 mG. Relatively low field strengths are found at 1665, 1667 and 1720 MHz in maser group *d* in the west of the region. It is generally assumed that the magnetic field is coupled to the gas in star-forming regions. In this case, models predicting different densities for emission from different lines must explain why magnetic fields are all so similar, because all the frequencies exhibit similar field distributions. While the overall density cannot vary much because of magnetic field implications, the OH abundance could still vary significantly.

A correlation was found between the magnetic field strength and total polarization, where masers of high magnetic field strength always displayed high total polarization. This is probably because the higher gas density, presumed to accompany higher magnetic field strength, enhances polarization. A correlation was also found at all four frequencies between the magnetic field strength and the size of the masers. This is an effect of 'magnetic beaming', which

could be enhanced by stronger fields. Because stronger fields would also indicate higher densities, a maser cloud of smaller size can become strong enough to be detected. An unexplained correlation was found between the degree of polarization and the FWHM of a maser, where masers with low total polarizations tended to have narrow linewidths.

A relationship was discovered between the Landé Zeeman line splitting factor and the likelihood that masers will be in a Zeeman pair, showing that larger Landé factors made it easier to destroy Zeeman pairs. This has major implications for theories that intend to explain the occurrence of uneven Zeeman pairs, and isolated Zeeman components. The general excess of LCP masers at 1665 MHz was shown unlikely to be a chance phenomenon, and so is probably indicative of a prevailing condition in the maser clouds that can affect Zeeman pair formation. The most likely candidate for this is velocity shifts in the masing gas.

All the ground-state masers show similar morphology, polarization, magnetic field and velocity distributions. However, instances of co-propagation of two maser frequencies are extremely rare, with instances of more than two lines not detected at all. A large portion of the total number of maser overlaps occur in the arc of maser emission in the south of the region, proposed to be tracing a shock. A propagating shock scenario is also proposed to account for near-overlaps between 1612- and 1665-MHz masers, where the 1612-MHz emission physically lies ∼40 au ahead of 1665-MHz emission in these shocks. The relative strengths of the lines co-propagating is of great importance to theoretical modellers, and the results obtained in this work show that, in strong contrast to the strength of emission from the region as a whole, the 1665-MHz emission is slightly weaker than the 1667-MHz emission. This will be a major constraint on future models.

ACKNOWLEDGMENTS

MMW thanks the Engineering and Physical Sciences Research Council (EPSRC) for funding him as a postgraduate student. We would like to thank the referee, Professor Mark Reid, for his comments that have helped us to improve this paper and Paper I. The NRAO is a facility of the National Science Foundation operated under cooperative agreement by Associated Universities Inc.

REFERENCES

Argon A. L., Reid M. J., Menten K. M., 2000, ApJS, 129, 159
Baudry A., Diamond P. J., 1991, A&A, 247, 551
Baudry A., Diamond P. J., 1998, A&A, 331, 697
Baudry A., Diamond P. J., Booth R. S., Graham D., Walmsley C. M., 1988, A&A, 201, 102
Bloemhof E. E., Reid M. J., Moran J. M., 1992, ApJ, 397, 500
Cook A. H., 1966, Nat, 211, 503
Desmurs J. E., Baudry A., Wilson T. L., Cohen R. J., Tofani G., 1998, A&A, 334, 1085
Elitzur M., Hollenbach D. J., McKee C. F., 1992, ApJ, 394, 221
Fouquet J. E., Reid M. J., 1982, AJ, 87, 691
Gaume R. A., Mutel R. L., 1987, ApJS, 65, 193
Gray M. D., Field D., Doel R. C., 1992, A&A, 262, 555
Gray M. D., Cohen R. J., Richards A. M. S., Yates J. A., Field D., 2001, MNRAS, 324, 643
Güsten R., Fiebig D., Uchida K. I., 1994, A&A, 286, L51
Lo K. Y., Walker R. C., Burke B. F., Moran J. M., Johnston K. J., Ewing M. S., 1975, ApJ, 202, 650
Lonsdale C. J., Lonsdale C. J., Diamond P. J., Smith H. E., 1998, ApJ, 493, 13
Mader G. L., Johnston K. J., Moran J. M., 1978, ApJ, 224, 115
Masheder M. R. W., Field D., Gray M. D., Migenes V., Cohen R. J., Booth R. S., 1994, A&A, 281, 871
McLeod G. C., 1997, MNRAS, 285, 635
Nedoluha G. E., Watson W. D., 1990, ApJ, 361, 653
Norris R. P., Booth R. S., 1981, MNRAS, 195, 213
Norris R. P., Booth R. S., Diamond P. J., 1982, MNRAS, 201, 209
Palmer P., Goss W. M., Devine K. E., 2003, ApJ, 599, 325
Thissen T., Spiecker H., Andresen R., 1999, A&AS, 137, 323
Wright M. M., 2001, PhD thesis, Univ. of Bristol
Wright M. M., Gray M. D., Diamond P. J., 2004, MNRAS, in press (doi:10.1111/j.1365-2966.2004.07572.x) (this issue) (Paper I)

This paper has been typeset from a TEX/LATEX file prepared by the author.